Rare Metal Materials and Engineering
Volume 55, Issue 1, January 2026
Available online at www.rmme.ac.cn

Science Press

Cite this article as: Li Long, Xiao Yichen, Shi Lei, et al. Numerical Simulation on Thermomechanical Coupling Process in Friction Stir-Assisted Wire Arc Additive Manufacturing[J]. Rare Metal Materials and Engineering, 2026, 55(01): 1-8. DOI: https://doi.org/10.12442/j.issn.1002-185X.20250286.

ARTICLE

Numerical Simulation on Thermomechanical Coupling Process in Friction Stir-Assisted Wire Arc Additive Manufacturing

Li Long[1], Xiao Yichen[2], Shi Lei[1,2], Chen Ji[2], Wu Chuansong[1,2]

[1] State Key Laboratory of Advanced Equipment and Technology for Metal Forming, Shandong University, Jinan 250061, China; [2] Key Laboratory for Liquid-Solid Structural Evolution and Processing of Materials, Ministry of Education, Shandong University, Jinan 250061, China

Abstract: Wire arc additive manufacturing (WAAM) has emerged as a promising approach for fabricating large-scale components. However, conventional WAAM still faces challenges in optimizing microstructural evolution, minimizing additive-induced defects, and alleviating residual stress and deformation, all of which are critical for enhancing the mechanical performance of the manufactured parts. Integrating interlayer friction stir processing (FSP) into WAAM significantly enhances the quality of deposited materials. However, numerical simulation research focusing on elucidating the associated thermomechanical coupling mechanisms remains insufficient. A comprehensive numerical model was developed to simulate the thermomechanical coupling behavior in friction stir-assisted WAAM. The influence of post-deposition FSP on the coupled thermomechanical response of the WAAM process was analyzed quantitatively. Moreover, the residual stress distribution and deformation behavior under both single-layer and multi-layer deposition conditions were investigated. Thermal analysis of different deposition layers in WAAM and friction stir-assisted WAAM was conducted. Results show that subsequent layer deposition induces partial remelting of the previously solidified layer, whereas FSP does not cause such remelting. Furthermore, thermal stress and deformation analysis confirm that interlayer FSP effectively mitigates residual stresses and distortion in WAAM components, thereby improving their structural integrity and mechanical properties.

Key words: friction stir processing; wire arc additive manufacturing; numerical simulation; thermomechanical coupling; temperature field; deformation

1 Introduction

Metal additive manufacturing (AM) technologies are experiencing rapid advancement and increasing adoption across high-performance industries, such as aerospace, marine, automobile, and biomedical applications[1]. Commonly used metal AM technologies include selective laser melting, selective electron beam melting, wire arc additive manufacturing (WAAM), electron beam freeform fabrication, and direct laser deposition[2]. Among these techniques, WAAM has emerged as a preferred method for fabricating large-scale components, due to its high deposition efficiency, low equipment costs, and high material utilization rate[3].

During WAAM, deposited materials undergo intricate thermophysical and metallurgical transformations. These phenomena generate substantial residual stresses and component distortions, compromising dimensional stability and mechanical properties. Such effects detrimentally influence the geometric precision and functional performance of fabricated parts[3]. Consequently, optimizing the material microstructure, reducing AM-induced defects, and mitigating residual stresses and deformations, all to improve the mechanical properties of the fabricated components, are critical research directions in metal AM. To date, achieving high-quality and efficient AM of large metal components

Received date: May 24, 2025
Foundation item: National Key Research and Development Program of China (2022YFB4600902); Shandong Provincial Science Foundation for Outstanding Young Scholars (ZR2024YQ020)
Corresponding author: Shi Lei, Ph. D., Professor, State Key Laboratory of Advanced Equipment and Technology for Metal Forming, Shandong University, Jinan 250061, Tel: 0086-531-88395987, E-mail: lei.shi@sdu.edu.cn

remains a significant challenge[4–6].

To address these challenges, global research efforts have been dedicated to advancing process control methodologies for AM. Prominent approaches include external field-assisted processing[7], ultrasonic in-situ strengthening[8], high-pressure rolling[9], and laser shock peening[10]. Among these methods, friction stir processing (FSP) has demonstrated remarkable effectiveness. The application of FSP to deposited layers induces microstructural refinement through severe plastic deformation, while simultaneously introducing beneficial compressive stresses. This thermomechanical treatment significantly enhances the material properties[11].

Consequently, numerous studies have explored the application of FSP to WAAM-fabricated components using various materials. Zhang et al[12] performed FSP on 2319 aluminum alloy fabricated by WAAM and observed a significant reduction in porosity and notable grain refinement. The tensile strength and elongation of the additive manufactured components increased by 10.6% and 158.6%, respectively. Similarly, He et al[13] applied FSP to 6061 aluminum alloy produced by WAAM, reporting that the grain size was reduced from 128 μm to 5 μm, and that the microhardness, yield strength, and tensile strength improved by 31.5%, 23.3%, and 6.0%, respectively.

In addition to post-processing approaches, researchers have also implemented in-situ FSP as an interlayer treatment during WAAM. This integrated approach enables concurrent microstructural modification and mechanical property enhancement throughout the deposition process. Guo et al[14] conducted interlayer FSP on Al-Zn-Mg-Cu-Sc-Zr alloy fabricated by WAAM, finding a significant reduction in porosity and grain refinement to approximately 1 μm in size. After the treatment, the alloy's strength, plasticity, and fatigue properties were all improved. Similarly, Dai et al[15] applied interlayer FSP to 2319 aluminum alloy WAAM components, leading to increases of 8.75%, 32.2%, and 20% in tensile strength, yield strength, and elongation, respectively. Compared to post-processing FSP, interlayer FSP enables in-situ control of geometry and mechanical properties during WAAM, thereby yielding superior performance enhancements.

However, the influence of post-treatment FSP on the thermomechanical coupling behavior during WAAM of steel remains unexplored. To address this gap, this study presents a numerical simulation of the thermomechanical coupling process in WAAM, accompanied by quantitative analysis of FSP post-treatment effects on the coupled thermal-stress evolution. The findings provide critical theoretical guidance for optimizing thermomechanical process control in WAAM and mitigating residual stresses and distortions in fabricated components.

2 Thermomechanical Coupling Numerical Model of AM Process

2.1 Geometry model and mesh division

In this study, Q235 low-carbon steel was selected as the substrate, with duplex stainless-steel wire (diameter: 1.2 mm) serving as the feedstock for WAAM. The deposition process incorporated oscillatory arc motion along the travel direction, ensuring symmetrical distribution of heat and material. To enhance computational efficiency, a symmetric model was employed, and the geometry of the additive layers was simplified to a rectangular prism based on the actual layer thickness in the AM process. This simplification was justified by the nearly planar top surface resulting from arc oscillation and subsequent FSP. The entire model was defined as a deformable solid, and the mirror-symmetric diagram of the single-layer additive model is shown in Fig.1. The dimensions of the cold metal transfer (CMT) substrate are as follows: length=300 mm, width=100 mm, and thickness=6 mm. The size of each additive layer is set to length=250 mm, width=30 mm, and layer height=3 mm.

A mesh sensitivity analysis was performed on the single-layer deposition model to optimize computational accuracy and efficiency. Numerical convergence was achieved when the element size in the deposition zone was set to 2 mm, as evidenced by the stabilization of peak temperature values. Subsequent mesh refinement beyond this threshold demonstrated marginal improvements in solution accuracy, while incurring disproportionate computational overhead. Thus, the final mesh size was set to 2.0 mm×1.5 mm×1.5 mm. The substrate and additive areas were meshed into 22 000 elements and 27 090 nodes, with all elements using a hexahedral eight-node mesh configuration. Mesh sensitivity results are summarized in Table 1.

2.2 Heat source model

In this study, Goldak's double ellipsoid heat source model was used to simulate the AM process. The expressions for the double ellipsoid heat source model are as follows:

$$q_1(x,y,z)=\frac{6\sqrt{3}\,f_1Q}{a_1bc\pi\sqrt{\pi}}\exp\left(-\frac{3z^2}{a}-\frac{3x^2}{b^2}-\frac{3y^2}{c^2}\right) \quad (1)$$

$$q_2(x,y,z)=\frac{6\sqrt{3}\,f_2Q}{a_2bc\pi\sqrt{\pi}}\exp\left(-\frac{3z^2}{a}-\frac{3x^2}{b^2}-\frac{3y^2}{c^2}\right) \quad (2)$$

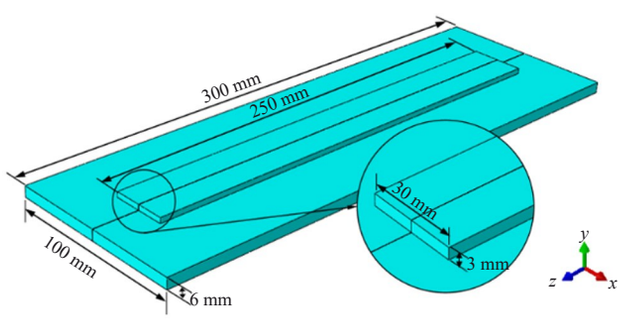

Fig.1 Mirror-symmetric diagram of single-layer additive model

Table 1 Calculation results of mesh sensitivity for different mesh sizes

Maximum size/mm	4	2	1
Peak temperature/°C	3 782.2	3 749.5	3 749.3
Calculation time/s	10 352	17 452	28 652

where q_1 and q_2 represent the heat flux density functions for the front and rear parts of the heat source, respectively; a_1, a_2, a, b, and c are the distribution parameters of the double ellipsoid heat source based on experimental results and empirical data during the calculation; f_1 and f_2 represent the heat input fractions for the front and rear parts of the heat source, respectively; Q is the effective power. Q can be given by:

$$Q = \eta UI \tag{3}$$

where η is the heat source efficiency, taken as 0.83[16]; U is the arc voltage; I is the additive current. The voltage and current values are aligned with the experimental parameters, which are specified as 14.6 V and 132 A, respectively. In this study, f_1 and f_2 are given by:

$$f_1 = \frac{2a_1}{a_1 + a_2} \tag{4}$$

$$f_2 = \frac{2a_2}{a_1 + a_2} \tag{5}$$

2.3 Boundary conditions

The numerical model incorporates coupled thermomechanical boundary conditions to accurately simulate the AM process. For thermal boundary conditions, conductive, convective, and radiative heat transfer mechanisms between the workpiece and the surrounding environment are considered. For mechanical boundary conditions, the structural constraints imposed by the clamping system and their influences on thermally induced stresses and deformations are modeled. The specific boundary conditions implemented in this study are defined as follows.

2.3.1 Thermal boundary conditions

The thermal model considers only conductive heat transfer within the workpiece and convective heat dissipation at the workpiece-environment interface. Radiation effects are neglected in this formulation to maintain computational efficiency, while still capturing the dominant heat transfer mechanisms. Heat conduction between the workpiece and the clamping device is omitted. During the WAAM process, heat conduction is governed by Fourier's law, expressed as follows:

$$\rho C_p \frac{\partial T}{\partial t} = \frac{\partial}{\partial x}\left(\lambda \frac{\partial T}{\partial x}\right) + \frac{\partial}{\partial y}\left(\lambda \frac{\partial T}{\partial y}\right) + \frac{\partial}{\partial z}\left(\lambda \frac{\partial T}{\partial z}\right) \tag{6}$$

where ρ is density; C_p is the specific heat capacity; T is transient temperature; t is time; λ is heat conduction coefficient. Convective heat transfer is primarily driven by the temperature difference between the workpiece and the environment, along with the convective heat transfer coefficient. Therefore, the thermal convection phenomenon is expressed by Newton's cooling law:

$$\frac{Q_c}{A} = -h\left(T_s - T_0\right) \tag{7}$$

where Q_c/A represents the heat convection loss per unit area; h is the convective heat transfer coefficient between the workpiece and air, taken as 50 W/(m^2·K) [17]; T_s is the temperature of the not-preheated workpiece with the initial temperature set to 20 ℃; T_0 is the ambient temperature around the workpiece set to 20 ℃.

2.3.2 Mechanical boundary conditions

The model incorporates symmetrical boundary conditions along the midplane to reduce computational complexity. Following completion of either the additive deposition or FSP operation, the mechanical constraints representing the clamping fixture are incrementally released. To ensure numerical stability of the solution during fixture removal and properly account for thermally-induced deformation effects, a two-point displacement constraint is implemented during the constraint release stage. This approach effectively prevents rigid body motion while maintaining solution accuracy for distortions in the heat-affected zone.

2.4 Modeling of FSP

In this study, a non-pinned flat-axis shoulder stir tool is used for interlayer FSP. To enhance computational efficiency, the surface morphology of the shoulder is neglected and simplified as a smooth surface. As shown in Fig. 2, the outer radius of the stir tool shoulder is R_1. A small segment with width dr is selected from this annular region. It is assumed that the stir tool rotates at an angular velocity ω, the friction coefficient between the tool and steel is μ, taken as 0.25[18], the downward pressure during FSP is F, r is the distance from the integration point on the welded plate surface to the center of the stir tool, and the surface pressure during processing is P. The frictional force df acting on the small segment with width dr is given by:

$$\mathrm{d}f = \mu F = \mu P \mathrm{d}s = \mu P r \mathrm{d}\theta \mathrm{d}r \tag{8}$$

where μ is frictional coeffcient; F is downward pressure; ds is local contact segment; r is radial distance between segment with the axial of FSP tool; θ is the angle between welding direction and r radius vector direction. The work done by the frictional force per unit time, i.e., the frictional heat power dq, is given by:

$$\mathrm{d}q = \omega r \mathrm{d}f = \mu P \omega r^2 \mathrm{d}\theta \mathrm{d}r \tag{9}$$

By integrating over this annular region, the total frictional heat Q_{tot} between the shoulder and the deposition layer surface can be obtained:

$$Q_{tot} = \int_0^{R_1} \mu P \omega r^2 \,\mathrm{d}r \int_0^{2\pi} \mathrm{d}\theta = \frac{2}{3}\pi \mu P \omega R_1^3 \tag{10}$$

Since the stir tool shoulder presses into the welded plate at a shallow depth, this portion of the heat source is treated as a

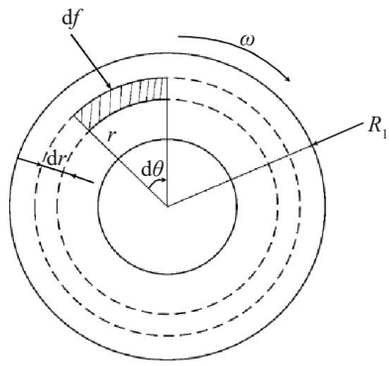

Fig.2 Schematic diagram of heat generation due to the contact between the stir tool shoulder and the workpiece

surface heat source. Based on the total heat generated as mentioned above, the heat flux density $q_f(r)$ at the contact interface between the shoulder and the deposition layer during FSP can be expressed as:

$$q_f(r) = \frac{\mu\eta NFr}{30R_1^2} \quad (0 \leqslant r \leqslant R_1) \tag{11}$$

where N is the rotational speed of the stir tool; η is the thermal efficiency. The heat source model described above is used to consider the thermomechanical coupling effect of FSP, with other boundary conditions being the same as those in the arc AM process.

3 Results and Discussion

3.1 Thermal process analysis of WAAM

A coupled thermomechanical finite element analysis was implemented to quantitatively characterize the transient temperature field evolution during WAAM. This numerical approach enables comprehensive investigation of the complex heat transfer phenomena and the associated thermal gradients inherent to the deposition process. Fig. 3 shows the temperature fields at three selected time instants: t=124 s, t=374 s, and t=624 s, which correspond to the middle times of the first, second, and third deposition layers in the WAAM, respectively.

Thermal field analysis reveals that the temperature distribution profiles exhibit consistent patterns across successive deposition layers, maintaining characteristics similar to those of the initial layer. However, progressive layer deposition induces a cumulative preheating effect: previously deposited layers elevate the thermal baseline of subsequent layers. This thermal accumulation phenomenon results in a systematic increase in substrate temperature as AM proceeds. Consequently, the volume of the molten pool in the additive region also increases.

A quantitative analysis of the thermal cycling characteristics was performed by extracting thermal histories from distinct through-thickness regions at the longitudinal centerline of the WAAM deposition layers. This methodology enables systematic investigation of the transient thermal profiles experienced during multilayer deposition. Fig. 4 shows the thermal cycles experienced by the central regions of different deposition layers during WAAM. It is evident that after the first deposition layer is completed, the temperature decreases rapidly. However, when the second deposition layer is added, the temperature at this location increases again, with the maximum temperature exceeding 1600 °C. This indicates partial remelting of the first layer during the deposition of the second layer. During the deposition of the third layer, the peak temperature reaches 1000 ° C, which does not exceed the remelting temperature of 1400 °C. The green line represents the thermal cycle at the center point of the second deposition layer, i. e., the point with coordinate (0, 3, 150). It can be observed that the thermal cycle curve follows a pattern similar to that of the first layer. During the deposition of the third layer, partial remelting of the second deposition layer also occurs. The blue line represents the thermal cycle at the center point of the third deposition layer, i. e., the point with coordinate (0, 6, 150). Comparative analysis of thermal cycles

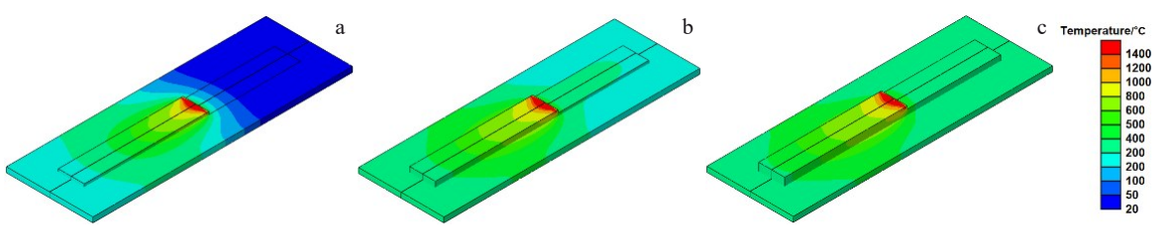

Fig.3 Temperature distributions at characteristic middle times of three-layer WAAM process: (a) t=124 s, first layer; (b) t=374 s, second layer; (c) t=624 s, third layer

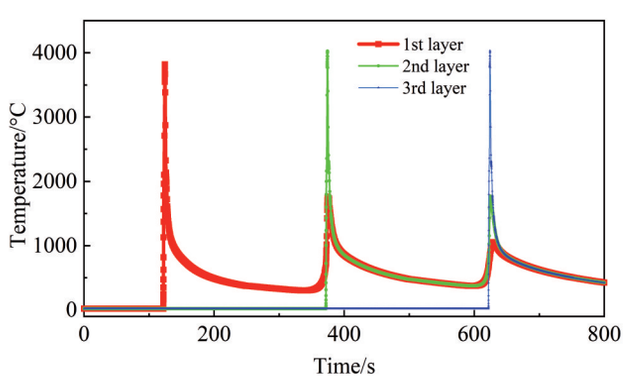

Fig.4 Temperature-time curve of characteristic points in three-layer WAAM

across successive deposition layers demonstrates that while the second and third layers exhibit comparable peak temperatures, both consistently exceed the maximum thermal excursion observed in the initial deposition layer. This thermal elevation trend provides empirical evidence of progressive heat accumulation with increasing layer count, resulting in systematically elevated peak temperatures during multilayer deposition.

3.2 Effect of interlayer FSP on temperature field in AM

A systematic investigation of the effects of interlayer FSP on the thermal field characteristics and cyclic thermal history in WAAM was conducted using a cylindrical FSP tool with a shoulder diameter of 24 mm. The processing parameters were precisely controlled with an advancing speed of 60 mm/min, a rotational velocity of 600 r/min, and an axial force of 5 kN to

ensure consistent thermomechanical conditions during layer-by-layer deposition. Fig. 5 shows the temperature fields at different time instants during the friction stir-assisted WAAM process. The first 350 s correspond to the temperature field of pure arc AM, which is the same as that described in Section 3.1, so no further analysis is needed. Only the temperature field after the interlayer FSP treatment is analyzed in this research. After t=350 s, which marks the completion of the first AM layer and the beginning of FSP, it can be observed that after the additive process, the maximum temperature during FSP is approximately 750 °C, which does not exceed the melting point of stainless steel, indicating that no remelting occurs.

The coordinate system is established, with the deposition initiation point defined as the origin (0, 0, 0) and the build direction aligned with the negative z-axis. Thermal histories are extracted at three strategically selected monitoring locations: (0, 0, −150), (0, 3, −150), and (0, 6, −150). These locations are used to characterize spatial temperature variations during deposition, as illustrated in Fig. 6. It can be observed that after the completion of AM deposition, the temperature of the additive layer decreases rapidly. As the FSP processing progresses, the temperature increases again, reaching a maximum of approximately 750 °C. During the subsequent deposition of the next layer, the temperature of the previous additive layer also rises and exceeds 1600 °C, which is above the melting point of stainless steel. However, during the deposition of the third deposition layer, the temperature does not exceed the melting point, indicating that the remelting phenomenon only occurs within the previously deposited additive layers.

3.3 Numerical simulation of stress in additively manufactured components

3.3.1 Stress analysis of arc-based additively manufactured component

Fig. 7 shows the distributions of Mises stress, lateral stress, and longitudinal stress at t=125 s during the deposition of the first layer of WAAM. It can be observed that the Mises stress is primarily concentrated in the additive layer. Lateral tensile stress is mainly distributed in the substrate, with concentration at the side edges of the substrate and a maximum value of approximately 275 MPa. The lateral compressive stress is mainly distributed at the middle of the initiation zone of the additive layer and the front side of the melt pool on thesubstrate. The longitudinal tensile stress is primarily distributed in the additive layer, while the longitudinal compressive stress is mainly distributed in the substrate, concentrated at the side edges of the substrate, with a maximum value of 256 MPa.

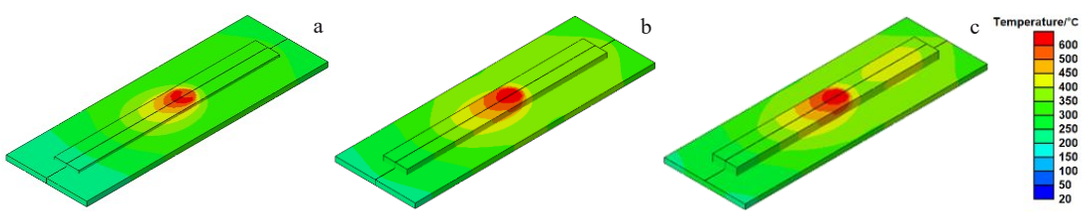

Fig.5 Temperature distributions at characteristic middle time of three-layer friction stir-assisted WAAM process: (a) t=350 s, first layer; (b) t=840 s, second layer; (c) t=1331 s, third layer

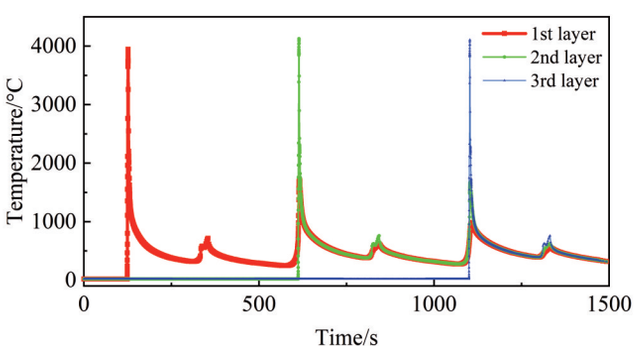

Fig.6 Temperature-time curve for characteristic points of three-layer friction stir-assisted WAAM

Fig. 8 shows the stress distribution of a three-layer additively manufactured component after cooling (t=3750 s). Fig. 8a represents the Mises equivalent stress of the additively manufactured component. It can be seen that after WAAM, the higher Mises stress is mainly concentrated in the additive layer, with a maximum value of approximately 420 MPa. Fig. 8b shows the lateral stress distribution in the additively manufactured component. It can be observed that the lateral tensile stress is primarily distributed in the substrate, with

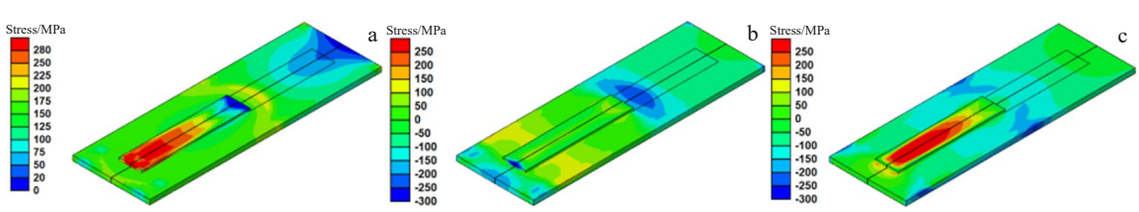

Fig.7 Stress distributions at middle time (t=125 s) of the first layer of WAAM: (a) Mises stress, (b) lateral stress, and (c) longitudinal stress

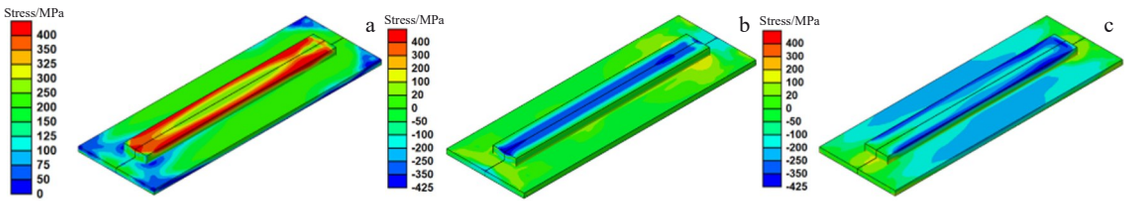

Fig.8 Stress distributions of three-layer WAAM after cooling and unloading (t=3750 s): (a) Mises stress, (b) lateral stress, and (c) longitudinal stress

localized stress concentration at the end of the additive layer. The lateral compressive stress is mainly distributed in the additive layer, with a maximum value of approximately 420 MPa. Fig. 8c shows the longitudinal stress distribution in the additively manufactured component. It can be seen that the longitudinal tensile stress is distributed at both ends of the substrate, with partial stress concentration in the center of the deposition layer. The longitudinal compressive stress is distributed at the interface between the deposition layer and the substrate, with a maximum value of approximately 340 MPa.

3.3.2 Effect of FSP on thermal residual stresses in arc additively manufactured component

To quantitatively assess the influence of FSP on thermal-induced residual stresses, a comparative stress analysis was performed between conventional WAAM specimens and friction stir-assisted WAAM components. A linear evaluation path was defined along the vertical centerline (y-axis) of each workpiece, extending from the deposition surface to the substrate interface. Von Mises stress distributions along this path were systematically extracted and compared across processing conditions, as presented in Fig.9.

The results demonstrate that post-deposition FSP induces a substantial reduction in residual stresses within the additively manufactured component. Quantitative analysis reveals a 21.3% decrease in the maximum von Mises stress, from approximately 400 MPa in the as-deposited condition to 315 MPa after FSP treatment. These results indicate that interlayer FSP treatment can effectively reduce residual stresses in WAAM components.

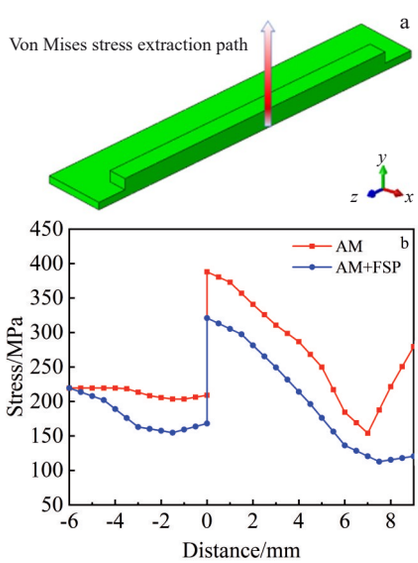

Fig.9 Schematic diagram of Von Mises stress extraction path (a); effect of interlayer FSP treatment on thermal-induced residual stress of WAAM component (b)

3.4 Numerical simulation of deformation in additively manufactured components

Fig. 10 shows the overall deformation of WAAM components with and without interlayer FSP treatment. Fig. 10a represents the deformation of a WAAM component without interlayer FSP treatment. It can be observed that after WAAM, both the substrate and the additive layer exhibit warping deformation, with larger deformation occurring near the end of the additive layer. The deformation at both ends is asymmetrical. Fig. 10b shows the deformation of a WAAM component with interlayer FSP treatment. Compared to Fig. 10a, it can be seen that after applying interlayer FSP, the overall deformation of the WAAM component decreases. The maximum deformation of the workpiece reduces from 4.8 mm to 3.3 mm. The above findings indicate that interlayer FSP treatment can significantly reduce the residual deformation in WAAM components, ensuring the forming accuracy of the components.

As evidenced in Fig. 10, the primary deformation mode of the additively manufactured component is out-of-plane warping. To quantify this behavior, a longitudinal evaluation path was defined along the substrate midplane (aligned with

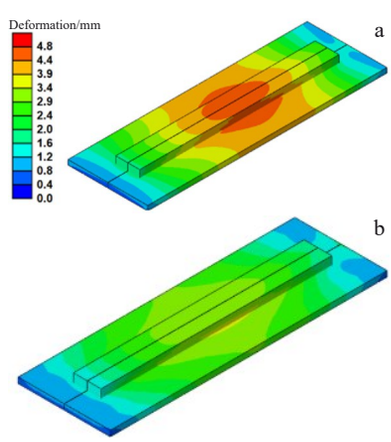

Fig.10 Deformation of WAAM component (a) and friction stir-assisted WAAM component (b)

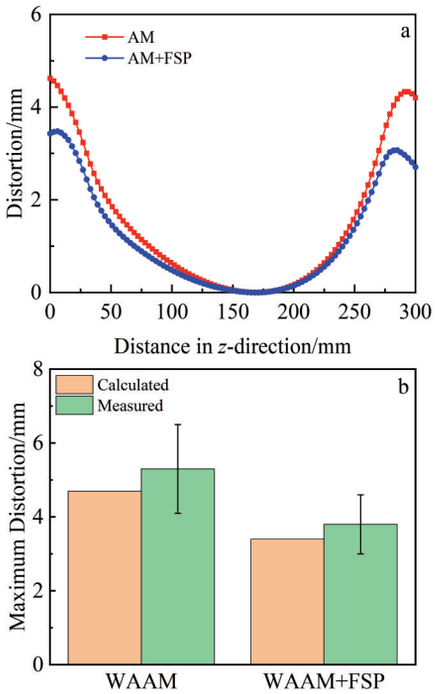

Fig.11 Predicted relative deformation in the *y*-direction (a) and comparison of the predicted maximum deformation with experimental results (b)

the deposition direction), and the vertical (*y*-axis) displacement field was analyzed. The computational predictions demonstrate strong agreement with experimental measurements, as validated by the comparative results presented in Fig.11. It can be seen that regardless of interlayer FSP treatment, the deformation distribution patterns of the additively manufactured component is generally the same, and the model-predicted relative deformation trend is in good agreement with that of the experimentally measured structure.

Thermomechanical analysis reveals that conventional three-layer WAAM deposition produces a maximum out-of-plane displacement of 5.0 mm in the fabricated component. In contrast, the implementation of interlayer FSP reduces this maximum deformation to 3.3 mm, corresponding to a 34% decrease in warpage magnitude. These results demonstrate that interlayer FSP effectively mitigates thermal-induced distortion during multilayer WAAM deposition through microstructural refinement and stress redistribution.

4 Conclusions

1) A thermomechanically coupled finite element model is developed to simulate WAAM, enabling the analysis of transient thermal profiles, stress evolution, and deformation behavior. Systematic evaluation of single- and multi-layer deposition processes reveals that while the second layer partially remelts the firstly solidified layer, the third layer's heat input only affects the second layer, due to progressive thermal accumulation. Subsequent depositions exhibit layer-limited remelting, with the heat exclusively penetrating the underlying layer immediately. This behavior stems from altered heat dissipation pathways, where prior deposited layers act as additional thermal mass, thereby localizing energy absorption. These findings quantitatively characterize the thermal penetration depth in multi-layer WAAM and its dependence on the deposition sequence.

2) Based on the WAAM model, a thermomechanical coupled numerical model for FSP is developed to analyze the thermal processes of the combined WAAM and FSP process. After FSP treatment, the maximum temperature in the additive layer is lower than that of the base material.

3) Within the WAAM process framework, the incorporation of FSP maintains the characteristic residual stress distribution profile while effectively mitigating stress magnitudes through thermomechanical coupling effects. FSP treatment reduces residual stresses in deposited components, with corresponding improvements in mechanical performance. These improvements are achieved without altering the fundamental stress distribution pattern established during WAAM deposition.

4) A comparative analysis is performed on WAAM components with and without interlayer FSP treatment. The results show that interlayer FSP effectively mitigates warpage deformation, reducing the maximum out-of-plane displacement by 34%. Specifically, for three-layer deposition, untreated WAAM components exhibit warpage of 5.0 mm, while FSP-treated specimens show a significantly reduced deformation of 3.3 mm. This improvement is attributed to FSP-induced microstructural refinement and residual stress release during layer-by-layer deposition.

References

1 Gu D, Shi X, Poprawe R *et al. Science*[J], 2021, 372(6545): 1487
2 Oliveira J P, Santos T G, Miranda R M. *Progress in Materials Science*[J], 2020, 107: 100590
3 Zhang H, Li R S, Liu J J *et al. Virtual and Physical Prototyping*[J], 2024, 19(1): e2390495
4 Chang Zijin, Zhang Ruize, Zeng Caiyou *et al. Rare Metal Materials and Engineering*[J], 2025, 54(3): 706 (in Chinese)
5 Li C D, Gu H M, Wang W *et al. Rare Metal Materials and Engineering*[J], 2020, 49(6): 1860
6 Lu Zhenyang, Liu Feng, Jiang Fan *et al. Rare Metal Materials and Engineering*[J], 2019, 48(2): 524 (in Chinese)
7 Ji F L, Hu Z Q, Qin X P *et al. Journal of Materials Science*[J], 2024, 59(33): 15920
8 Wang D Q, Wang Y J, Liu W H *et al. International Journal of Heat and Mass Transfer*[J], 2021, 180: 121790
9 Colegrove P A, Coules H E, Fairman J *et al. Journal of Materials Processing Technology*[J], 2013, 213(10): 1782
10 Li X L, Zhang L Q, Su Y *et al. Journal of Manufacturing Processes*[J], 2024, 126: 74
11 Lin Chunfa, Dai Yuxuan, Han Yuqiang *et al. Materials China*[J], 2024, 43(10): 944 (in Chinese)
12 Zhang X J, He Y R, Wei Y H. *CIRP Journal of Manufacturing*

Science and Technology[J], 2023, 46: 230
13 He P, Bai X W, Zhang H O. *Materials Letters*[J], 2023, 330: 133365
14 Guo X P, Ni D R, Li H J *et al. Journal of Materials Processing Technology*[J], 2023, 322: 118173
15 Dai G Q, Xue M H, Guo Y H *et al. Journal of Alloys and Compounds*[J], 2023, 968: 171781
16 Gupta D K, Mulik R S. *Progress in Additive Manufacturing*[J], 2025, 10(1): 631
17 Yang Nan. *Finite Element Numerical Simulation of Residual Stress in Shipbuilding Steel Components Manufactured by Arc Welding and Fused Deposition Modeling*[D]. Shenyang: Shenyang Aerospace University, 2023 (in Chinese)
18 Geng P H, Ma Y W, Ma N S *et al. International Journal of Machine Tools and Manufacture*[J], 2022, 174: 103858

搅拌摩擦辅助电弧增材制造热力耦合过程的数值模拟

李　龙[1]，肖亦辰[2]，石　磊[1,2]，陈　姬[2]，武传松[1,2]
(1. 山东大学 金属成形高端装备与先进技术全国重点实验室，山东 济南 250061)
(2. 山东大学 液固结构演变与材料加工教育部重点实验室，山东 济南 250061)

摘　要：电弧增材制造（WAAM）已成为大型构件成形制造的重要方法。但传统WAAM仍面临着如何改善材料微观组织、减少增材缺陷、降低工件残余应力和变形的问题，从而提升增材构件的力学性能。在WAAM过程中，进行层间搅拌摩擦处理可以调控构件的成形质量，但目前仍缺乏相关的热力耦合数值模拟研究。为此，建立了搅拌摩擦辅助WAAM热力耦合过程的数值模拟，定量分析了搅拌摩擦后处理对WAAM热力耦合过程的影响规律，分析了单层增材与多层增材过程中，搅拌摩擦处理对增材结构的残余应力与变形的影响规律。对WAAM和搅拌摩擦辅助WAAM不同沉积层的热过程进行分析。结果表明，进行后一层沉积会使已凝固的上一层发生局部重熔，而搅拌摩擦处理不会引起局部重熔。对增材构件进行热应力与变形分析，发现层间搅拌摩擦可以大大降低电弧增材构件的残余应力和翘曲变形，改善增材构件的性能。

关键词：搅拌摩擦处理；电弧增材制造；数值模拟；热力耦合；温度场；变形

作者简介：李　龙，男，1991年生，博士，山东大学金属成形高端装备与先进技术全国重点实验室，山东 济南 250061，E-mail：lli@mail.sdu.edu.cn